Charge exchange in collisions of beryllium with its ion

PCCP

Cite this: *Phys. Chem. Chem. Phys.*, 2011, **13**, 19026–19035

www.rsc.org/pccp

PAPER

Charge exchange in collisions of beryllium with its ion

Peng Zhang,[a] Alexander Dalgarno,[a] Robin Côté[b] and Enrico Bodo*[c]

Received 10th May 2011, Accepted 4th July 2011
DOI: 10.1039/c1cp21494b

Close-coupling calculations of the resonance and near resonance charge exchange in ion–atom collisions of Be_2^+ at low and intermediate energies are presented. Accurate *ab initio* calculations are carried out of the Born–Oppenheimer potentials and the non-adiabatic couplings that are due to the finite nuclear masses and drive the near resonance charge exchange. We show that the near resonance charge exchange cross section follows Wigner's threshold law of inelastic processes for energies below 10^{-8} eV and that the zero temperature rate constant for it is 4.5×10^{-10} cm^3 s^{-1}. At collision energies much larger than the isotope shift of the ionization potentials of the atoms, we show that the near resonance charge exchange process is equivalent to the resonance charge exchange with cross sections having a logarithmic dependence. We also investigate the perturbation to the charge exchange process due to the non-adiabatic interaction to an electronic excited state. We show that the influence is negligible at low temperatures and still small at intermediate energies despite the presence of resonances.

I. Introduction

The possibility of creating small ensembles of ultracold atoms and molecules has opened new research in physics and chemistry.[1–3] The recent experimental production of ultracold molecular ions[4–7] provides new opportunity for exploring ion–atom interactions[8,9] and collisional dynamics.[10–15] Of particular interest of cold molecular ions are novel applications to mass spectrometry, chemistry, and spectroscopy;[16] the implementation of scalable quantum-computation architecture;[17–19] the precision measurement tests of fundamental physics;[20] a better understanding of polaron physics;[21] the charge transport at low temperature[22] and producing ion–atom bound states to study many-body physics.[23]

The properties of the low-energy scattering states as well as those bound states near the dissociation thresholds depend ultimately on the long range part of the potential. The typical atom–ion interaction, asymptotically, has a R^{-4} dependence on distance and therefore decays more slowly than the van der Waals interaction between neutral atoms. Because of this strong polarization potential, the collision dynamics exhibits unique features both at low and high energies.[8–12,24] An atom–ion collision can lead to a charge exchange process which generally is an inelastic process when two different atoms are involved but is resonant when the two atoms are the same. In collisions of a positive ion with its parent atom of the same isotopic composition the identity of the nuclei must be taken into account and charge transfer collisions

$$A + A^+ \rightarrow A^+ + A$$

cannot be distinguished in principle from elastic collisions

$$A + A^+ \rightarrow A + A^+.$$

This charge exchange process has been studied theoretically and the cross sections are governed by the difference between the interaction potentials of the gerade and ungerade symmetry of the molecular ions A_2^+. Explicit examples include the calculations for $Na + Na^+$[10] and $Yb + Yb^+$.[13] Analysis of the differential cross sections has shown that, in the relatively high energy regime, peaks in the forward direction arise from elastic collisions and those in the backward direction from charge transfer.[13]

In the case of identical atoms, but with different isotopic composition, we have shown[11,12] that the charge transfer reaction becomes inelastic (near resonant process). This inelastic process is driven by the small non-adiabatic couplings between the two electronic states that are due to the small kinematic effects because of the finite nuclear mass. When different isotopes are involved, there occurs a change in the kinetic energies of the particles in the charge transfer collisions and not in the elastic collisions. The molecular u–g symmetry is broken and the molecular states separate at large internuclear distances to asymptotic binding energies for $A + A'^+$ and for $A^+ + A'$, differing by a small amount ΔE that depends on the masses and, to a smaller extent, on the electronic wavefunction. The Born–Oppenheimer (BO)

[a] *Institute for Theoretical Atomic and Molecular Physics (ITAMP), Harvard-Smithsonian Center for Astrophysics, Cambridge, MA 02138, USA*
[b] *Department of Physics, U-3046, University of Connecticut, Storrs, Connecticut 06269, USA*
[c] *Department of Chemistry, University of Rome "Sapienza", Rome, Italy. E-mail: bodo@caspur.it*

approximation fails because its symmetry properties are determined by the electronic Hamiltonian. We have explicitly dealt with such a case in our previous studies of the HD^+ [11] and Li_2^+ [12] molecular ions. While in the former we have used an analytical resolution of the one-particle Hamiltonian, in the latter we have devised a scheme for calculating by means of *ab initio* methods the rather weak couplings due to non-BO corrections using a MCSCF/MRCI framework.

We have also shown that the difference between the collision of identical isotopes (the resonant charge transfer) and that with isotopic exchange (near resonant charge transfer) is small for high collision energies, but becomes significantly larger at low energy. In the ultra-low energy limit, while a resonant charge transfer process has a constant cross section and the corresponding rate coefficient goes to zero, the near resonant, inelastic process has a diverging cross section. At energies much larger than ΔE, the scattering can be described by an elastic two-state approximation for which the direct coupling arising from the difference in nuclear masses is neglected,[11,12] and the charge exchange is governed largely by the difference between the two potentials.

As interest in the cold ion–atom collision is increasing, we have extended our efforts to the Be_2^+ molecular ion. A distinct and interesting feature arises because a third state, $B^2\Pi$, is involved in the collision process even at very low scattering energies since it crosses the two lowest Σ states in the inner regions of their potential wells. The non-adiabatic interaction between the Σ and Π states is weak, but nonetheless, we shall show that it does have an effect on the dynamics. Therefore, we believe that the work we present here goes well beyond a mere extension of our previous calculations to another mass combination and adds an interesting new element to the picture that may help in understanding the effects of this small non-adiabatic perturbation to collision processes governed by a strong polarization potential and to the prototypical two-state description of the charge exchange.

II. Collision dynamics

We consider the ion–atom collisions between Be^+ and Be, which may be the same or different isotopes. Their nuclear masses are labeled as m_a and m_b. After the separation of the kinetic energy operator of the center of nuclear mass (CNM) motion of the total system, the Hamiltonian of the entire system in the body fixed frame[25] is

$$H = T_N + T_e + T_{mp} + V_{int}(\mathbf{r}, \mathbf{R}), \quad (1)$$

where T_N is the kinetic energy operator for the relative motion of the nuclei, T_{mp} is the mass polarization term, T_e is the electron kinetic energy, $\mathbf{R}$ is the vector connecting the colliding nuclei, $\mathbf{r}$ measures the coordinates of electrons in the CNM frame, and $V_{int}(\mathbf{r}, \mathbf{R})$ contains all the electrostatic interactions. Combining $V_{int}(\mathbf{r}, \mathbf{R})$ and T_e yields the non-relativistic BO electronic Hamiltonian H_{el}, whose eigenstate and the corresponding eigenvalue are labeled collectively as $\psi(r; R)$ and ε. For the state α, $H_{el}\psi_{\alpha\Lambda}(r; R) = \varepsilon_\alpha\psi_{\alpha\Lambda}(r; R)$ with Λ being the projection of electronic orbital angular momentum onto the molecular axis. The mass polarization term reads

$$T_{mp} = -\frac{1}{2m}\sum_{i,j=1}^{N_e}\nabla_i\nabla_j, \quad (2)$$

where $m = m_a + m_b$ is the total nuclear mass and summation runs over the number of electrons N_e. Atomic units are used throughout the paper. The matrix element of T_{mp} between BO eigenstates $\psi_\alpha(r; R)$ and $\psi_\beta(r; R)$ is denoted as $\varepsilon_{\alpha\beta}^{mp}$. This matrix is symmetric, and asymptotically, the two diagonal matrix elements are the same for the $\tilde{X}^2\Sigma_g^+$ and $B^2\Sigma_u^+$ states.

The total wave function of the colliding system can be expanded as a sum of terms $\Psi^{J,M}(\mathbf{r}, \mathbf{R})$, characterized by the total angular momentum quantum number J and its projection M. Each $\Psi^{J,M}(\mathbf{r}, \mathbf{R})$ in the BO basis can be expressed as

$$\Psi^{J,M}(\mathbf{r}, \mathbf{R}) = e^{iM\varphi}\sum_{\alpha,\Lambda}\frac{1}{R}\chi_{\alpha\Lambda}^J(R)\Theta_{M,\Lambda}^J(\vartheta)\psi_{\alpha\Lambda}(r; R), \quad (3)$$

where ϑ and φ are the spherical angles of vector $\mathbf{R}$, $\Theta_{M,\Lambda}^J(\vartheta)$ is a generalized spherical harmonic, and $\chi_{\alpha\Lambda}^J(R)$ describes the radial motion of the nuclei.

Substituting expansion (3) into the time-independent Schrödinger equation and integrating out the electronic coordinates, we obtain a set of coupled equations for the radial functions $\chi^J(R)$ in the BO representation at the total energy E[26–28]

$$\begin{aligned}
&\left[-\frac{1}{2\mu}\frac{d^2}{dR^2} + \varepsilon_\alpha + \frac{J(J+1)-\Lambda^2}{2\mu R^2} - E\right]\chi_{\alpha\Lambda}^J \\
&= +\frac{1}{\mu}\sum_{\beta\neq\alpha}\left\langle\psi_\alpha\left|\frac{\partial}{\partial R}\right|\psi_\beta\right\rangle\frac{d\chi_{\beta\Lambda}^J}{dR} + \frac{1}{2\mu}\sum_\beta\left\langle\psi_\alpha\left|\frac{\partial^2}{\partial R^2}\right|\psi_\beta\right\rangle\chi_{\beta\Lambda}^J \\
&\quad - \frac{1}{2\mu R^2}\sum_\beta\left\langle\psi_\alpha\left|\hat{L}_x^2 + \hat{L}_y^2\right|\psi_\beta\right\rangle\chi_{\beta\Lambda}^J - \sum_\beta\varepsilon_{\alpha\beta}^{mp}\chi_{\beta\Lambda}^J \\
&\quad + \frac{1}{\mu R^2}\sum_\beta\sqrt{(J+\Lambda+1)(J-\Lambda)}\langle\psi_\alpha|i\hat{L}_y|\psi_\beta\rangle\chi_{\beta\Lambda+1}^J \\
&\quad - \frac{1}{\mu R^2}\sum_\beta\sqrt{(J-\Lambda+1)(J+\Lambda)}\langle\psi_\alpha|i\hat{L}_y|\psi_\beta\rangle\chi_{\beta\Lambda-1}^J,
\end{aligned} \quad (4)$$

where μ is the reduced mass of the system, and $\hat{L}_x$ and $\hat{L}_y$ are the x and y components of the electronic orbital angular momentum operator. We define

$$\begin{aligned}
F_{\alpha\beta} &= \frac{1}{\mu}\left\langle\psi_\alpha\left|\frac{\partial}{\partial R}\right|\psi_\beta\right\rangle \\
V_{\alpha\beta} &= \varepsilon_{\alpha\beta}^{mp} - \frac{1}{2\mu}\left\langle\psi_\alpha\left|\frac{\partial^2}{\partial R^2}\right|\psi_\beta\right\rangle + \frac{1}{2\mu R^2}\langle\psi_\alpha|\hat{L}_x^2 + \hat{L}_y^2|\psi_\beta\rangle \\
L_{\alpha\beta} &= \frac{1}{\mu R^2}[\sqrt{(J+\Lambda+1)(J-\Lambda)}\langle\psi_\alpha|i\hat{L}_y|\psi_\beta\rangle \\
&\quad - \sqrt{(J-\Lambda+1)(J+\Lambda)}\langle\psi_\alpha|i\hat{L}_y|\psi_\beta\rangle]
\end{aligned} \quad (5)$$

Eqn (4) can be written in a matrix form

$$\left[\mathbf{I}\frac{\mathrm{d}^2}{\mathrm{d}R^2}+2\mu\mathbf{F}\frac{\mathrm{d}}{\mathrm{d}R}+2\mu\mathbf{E}-2\mu\left(\mathbf{I}\frac{J(J+1)-\Lambda^2}{2\mu R^2}+\mathbf{e}+\mathbf{V}-\mathbf{L}\right)\right]\boldsymbol{\chi}=0, \tag{6}$$

with **I** being the identity matrix. In the present study, three BO states are included in eqn (6) and they are $\tilde{X}^2\Sigma_u^+$, $B^2\Sigma_g^+$, and $A^2\Pi_u$. The *g* and *u* symmetry disappear in the case of isotopic combination. The 2s → 2p transition of Be is 2.72 eV. For collisions at low temperatures, the contributions from the other molecular states formed by $Be^+(^2S)$ + $Be(^3P)$ are negligible.

F and **L** matrices have only off-diagonal elements and approach zero asymptotically in the BO representation (see discussion in Section III). The matrix **V** originates from the nuclear kinetic operator and the mass polarization term. Its diagonal elements are an adiabatic correction to the BO states. The off-diagonal elements couple the two Σ^+ states, and asymptotically separates the isotopic combinations of Be_2^+ to the correct limit of $\pm\frac{1}{2}\Delta E$. This asymptotic property can be easily understood by re-writing **V** in a Hermitian form

$$\tilde{V}_{\alpha\beta}=V_{\alpha\beta}-\frac{1}{2}\frac{\mathrm{d}}{\mathrm{d}R}F_{\alpha\beta}. \tag{7}$$

Eqn (7) is obtained by symmetric and anti-symmetric combinations of the matrix elements of the nuclear kinetic operator

$$\tilde{V}_{\alpha,\beta}=\tfrac{1}{2}[\langle\psi_\alpha|T_N|\psi_\beta\rangle+\langle\psi_\beta|T_N|\psi_\alpha\rangle], \tag{8}$$

and

$$\frac{\partial}{\partial R}F_{\alpha\beta}=\langle\psi_\alpha|T_N|\psi_\beta\rangle-\langle\psi_\beta|T_N|\psi_\alpha\rangle. \tag{9}$$

Eqn (9) is obtained by differentiating $F_{\alpha\beta}$ and $F_{\beta\alpha}$.

Asymptotically, eqn (6) remains coupled. The proper scattering boundary conditions can be restored by transforming the radial wave functions associated with the Σ^+ states into an atomic representation. This is achieved by addition and subtraction of the two coupled equations in eqn (6), and the resulting equation is

$$\left[\mathbf{I}\frac{\mathrm{d}^2}{\mathrm{d}R^2}+2\mu\mathbf{F}\frac{\mathrm{d}}{\mathrm{d}R}+2\mu\mathbf{E}-2\mu\left(\mathbf{I}\frac{J(J+1)-\Lambda^2}{2\mu R^2}+\mathbf{C}\right)\right]\boldsymbol{\zeta}=0. \tag{10}$$

Here $\zeta_1=\chi_1+\chi_2$, $\zeta_2=\chi_2-\chi_1$, and $\zeta_3=\chi_3$. The numbers 1, 2, and 3 associated with χ label the $\tilde{X}^2\Sigma^+$, $B^2\Sigma^+$, and $A^2\Pi$ states, respectively. The **C** matrix is

$$\mathbf{C}=\begin{pmatrix}\varepsilon^+-\tilde{V}^+-\tilde{V}_{12} & \varepsilon^--\tilde{V}^--\frac{1}{2}F_{12} & -\frac{\sqrt{J(J+1)}}{R^2}(L_{13}+L_{23})\\ \varepsilon^--\tilde{V}^-+\frac{1}{2}F_{21} & \varepsilon^+-\tilde{V}^++\tilde{V}_{21} & -\frac{\sqrt{J(J+1)}}{R^2}(L_{23}-L_{13})\\ \frac{\sqrt{J(J+1)}}{2R^2}(L_{31}+L_{32}) & \frac{\sqrt{J(J+1)}}{2R^2}(L_{32}-L_{31}) & \varepsilon_3\end{pmatrix}, \tag{11}$$

where $\varepsilon^+=\frac{1}{2}(\varepsilon_1+\varepsilon_2)$, $\varepsilon^-=\frac{1}{2}(\varepsilon_2-\varepsilon_1)$, $\tilde{V}^+=\frac{1}{2}(\tilde{V}_{11}+\tilde{V}_{22})$, and $\tilde{V}^-=\frac{1}{2}(\tilde{V}_{22}-\tilde{V}_{11})$.

Solutions to eqn (10) are obtained through a modified Numerov propagator that accounts for the linear derivative term.[11,29] The scattering **S** matrix is derived in the asymptotic region from the radial function $\boldsymbol{\zeta}(R)=\mathbf{J}(R)-\mathbf{N}(R)\mathbf{K}$, where $\mathbf{J}(R)$ and $\mathbf{N}(R)$ are matrices of the Riccati-Bessel and Riccati-Neumann functions.[30] $\mathbf{S}=(\mathbf{I}+i\mathbf{K})^{-1}(\mathbf{I}-i\mathbf{K})$. The charge exchange and the elastic cross sections can then be expressed as

$$\sigma_{cx}(\alpha\rightarrow\beta)=\frac{\pi}{k_\alpha^2}\sum_J(2J+1)|S^J_{\alpha\beta}|^2 \tag{12}$$

and

$$\sigma_{el}(\alpha\rightarrow\alpha)=\frac{\pi}{k_\alpha^2}\sum_J(2J+1)|1-S^J_{\alpha\alpha}|^2, \tag{13}$$

where k_α is the wave vector of the channel α. Nuclear masses of 9.0121822 and 10.0135338 were used in the calculation.

III. Electronic structure calculations of Born–Oppenheimer potentials and couplings

A Born–Oppenheimer potentials

The interaction potentials of the Be_2^+ molecular ion have been examined theoretically by several groups.[31–33] The ro-vibrational structure of the ground electronic state, $\tilde{X}^2\Sigma_u^+$, has been characterized experimentally using the pulsed-field ionization zero kinetic energy photoelectron technique.[34] Similar to H_2^+ and Li_2^+, the low energy ion–atom collisions are effectively governed by two molecular potentials, $\tilde{X}^2\Sigma_u^+$ and $B^2\Sigma_g^+$. However, at short internuclear distances the potential of the $A^2\Pi_u$ state, which originates from the asymptote $Be^+(^2S)$ + $Be(^3P)$, undergoes a rapid decrease and crosses both of the Σ states.[31] In the case of the scattering of different isotopes, this $^2\Pi$ state interacts with the Σ states, and consequently, in principle, it could modify the collision dynamics at low temperatures. In addition, the potential of the $B^2\Sigma_g^+$ state has a double minimum, which results from an avoided crossing with an upper state of the same symmetry.

To obtain a consistent description of these BO states and their interactions, the calculations of the three corresponding BO potentials were performed with the internally contracted multi-reference configuration interaction with singles and doubles (MRSDCI)[35] plus the multireference version of the Davidson correction (Q).[36] The reference wave functions of the MRCISD(Q) calculations are derived from a state-average multiconfiguration self-consistent field (MCSCF) approach,[37] in which the active space is formed by seven electrons in ten molecular orbitals (MOs) and the average includes all the six doublet states correlated to the $Be^+(^2S)$ + $Be(^3P)$ and $Be^+(^2S)$ + $Be(^1S)$ asymptotes with equal weights. The ten MOs come from the linear combination of 1s2s2p atomic

orbitals of Be, and the seven electrons are all the electrons of Be_2^+. The scalar relativistic effects were also included in our calculation by means of the third-order Douglas–Kroll–Hess Hamiltonian (DKH3).[38] DK-contracted augmented polarized weighted core/valence quintuple and quadruple zeta basis sets[39] (aug-cc-pwCVQZ and aug-cc-pwCV5Z) were used in the calculations. The final $\tilde{X}^2\Sigma_g^+$, $B^2\Sigma_u^+$ and $A^2\Pi_u$ potentials were obtained by extrapolating to the complete basis set limit (CBS) through[40]

$$V(n) = V_{\mathrm{CBS}} + \frac{B}{(n+1/2)^4}. \qquad (14)$$

The resulting CBS *ab initio* points for the two Σ states were fitted to the following analytical expression

$$V(R) = e^{-\beta R}\left(\sum_i a_i R^i\right) - \sum_{n=4,6,8} \frac{f_n(\beta R) C_n}{R^n}, \qquad (15)$$

where f_n is a damping function[41] and the dispersion coefficients, in atomic units, are $C_4 = 18.88$, $C_6 = 270.7$, and $C_8 = 1890.5$ a.u. The coefficient C_4 is half of the dipole polarizability of the beryllium atom.[42] C_6 is half of the quadrupole polarizability of Be,[42] to which we added 120.4 a.u. for the contribution of the ion–atom Be–Be^+ van der Waals interaction. This contribution is estimated from the Casimir–Polder equation, in which the frequency-dependent dipole polarizabilities of Be^+ were evaluated using the linear response coupled-cluster theory (LR-CCSD)[43] as implemented in NWCHEM 6.0[44] with a doubly augmented (d-aug-cc-pwCV5Z) basis set, and those for Be were taken from ref. 42. The coefficient C_8 is half of the octupole polarizability of Be.[42] These dispersion coefficients were held fixed in the fitting.

For the $A^2\Pi_u$ state we used an analogous expression. The long range part is given by

$$V_{\mathrm{LR}}(R) = -\sum_{n=3,4} \frac{f_n(\beta R) C_n}{R^n}. \qquad (16)$$

The leading interaction is a permanent quadrupole-charge interaction which is followed by the induced-dipole charge interaction. The quadrupole moment extracted from the fitting of the *ab initio* points is 4.20 a.u., which agree well with the theoretical values of ~4.54 a.u.[45,46] The fourth order term corresponds to the dipole polarizability of Be(^{3}P). Our fitting yields 38.0 a.u., which is in close agreement with the theoretical value of 39.04 a.u.[45]

The computed BO potentials are shown in Fig. 1, and the corresponding spectroscopic constants are reported in Tables 1 and 2 for the ground and excited states, respectively. Comparisons with the available experiment and representative theoretical results are also listed. The spectroscopic constants of the $\tilde{X}^2\Sigma_u^+$ state agree closely with experiment[34] and a recent high-level theoretical analysis.[33] For the $B^2\Sigma_g^+$ state, a double minimum is found in our calculations. D_e of the inner potential well is about 75 cm^{-1} smaller than a recent theoretical

Table 1 Spectroscopic constants of the $\tilde{X}^2\Sigma_u^+$ state of Be_2^+

	D_e (cm^{-1})	R_e/Å	$\omega_e{}^a$/cm^{-1}	$\omega_e x_e{}^a$/cm^{-1}
This work	16 472	2.221	527.4 (500.4)^b	4.49 (4.05)^b
Exp.[34]	16 438	2.211	525.88	4.44
Theory[33]	16 434	2.223	525.299	4.454
Theory[31]	15 889	2.231	502	4.2

^{a} ω_e and $\omega_e x_e$ were fitted using the first 7 vibrational levels according to $E(\nu) = \omega_e\nu - \omega_e x_e \nu(\nu+1)$, the same procedure as in Exp.[34] ^{b} Numbers with and without parentheses were calculated for ^{10}Be and ^{9}Be, respectively.

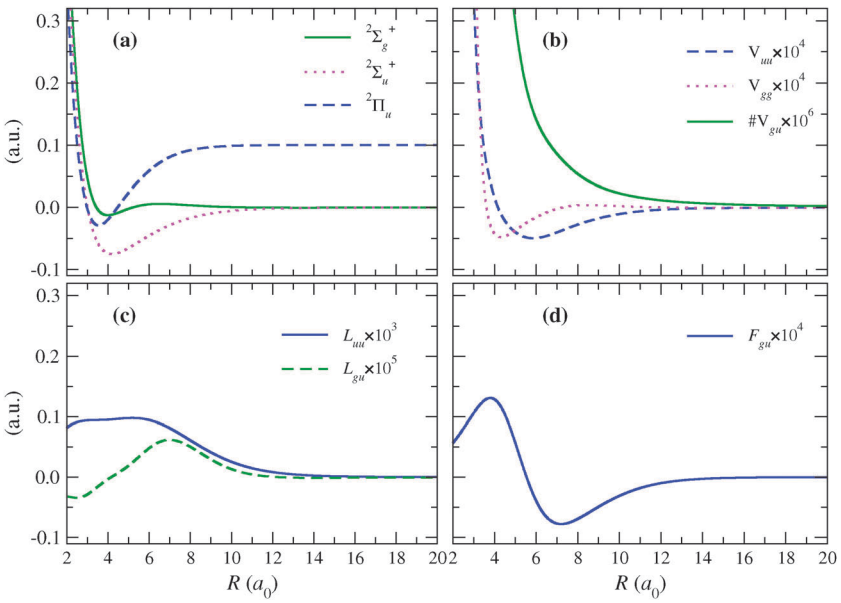

Fig. 1 The potential energy curves, adiabatic corrections and nonadiabatic couplings of the $\tilde{X}^2\Sigma_u^+$, $B^2\Sigma_g^+$ and $A^2\Pi_u$ as functions of internuclear distance R. The g and u symmetries are labeled according to the center of charge. (a) BO potentials; (b) $\tilde{V}_{\alpha\beta}$ between the two $^2\Sigma^+$ states; (c) the L_y couplings of $\tilde{X}^2\Sigma_u^+$–$A^2\Pi_u$ and $B^2\Sigma_g^+$–$A^2\Pi_u$; and (d) the first derivative coupling $F_{\alpha\beta}$.

Table 2 Spectroscopic constants of the $B^2\Sigma_g^+$ and $A^2\Pi_u^+$ states of $^9Be_2^+$

State		D_e/cm^{-1}	R_e/Å	ω_e/cm^{-1}	$\omega_e x_e$/cm^{-1}	T_0/cm^{-1}	R_c/Å (E_c/cm^{-1})[a]
$B^2\Sigma_g^+$ (inner well)	This work	2745	2.114	544	13.7	13 730	2.222 (−2557)[b]
	Theory[33]	2820.8	2.123	547.452	11.681	—	—
	Theory[31]	3145	2.128	517	13.2	13 953	—
	Theory[32]	2358	2.140	—	—	—	—
$B^2\Sigma_g^+$ (outer well)	This work	79.7	7.100	18.2	1.13	—	—
	Theory[33]	85.0	7.106	33.703	3.548	—	—
$A^2\Pi_u^+$	This work	28 354	1.878	859	6.9	10 266	—
	Theory[31]	26 858	1.882	818	6.2	11 017	1.615 (−1746)[c]
	Theory[32]	27 989	1.887	—	—	—	—

[a] R_c is the internuclear distance where two state cross and E_c is the potential energy at R_c relative to Be(^{1}S) + Be$^+$(^{2}S). [b] The crossing between $B^2\Sigma_g^+$ and $A^2\Pi_u^+$. [c] The crossing between $\tilde{X}^2\Sigma_u^+$ and $A^2\Pi_u^+$.

value of 2821 cm^{-1}.[34] Values for the outer well are in good agreement. The potential maximum is located at R = 3.452 Å, and the corresponding potential energy relative to the dissociation limit is 1260.3 cm^{-1}.

The $A^2\Pi_u$ state shows a deep potential minimum. The computed potential depth is about 1500 cm^{-1} deeper than those of previous calculations, and the potential minimum at R = 1.878 Å lies 6369 cm^{-1} below the Be(^{1}S) + Be$^+$(^{2}S) limit. $A^2\Pi_u$ crosses both of the $\tilde{X}^2\Sigma_u^+$ and $B^2\Sigma_g^+$ states near its potential equilibrium distance. The crossing with $\tilde{X}^2\Sigma_u^+$ is located at R = 1.615 Å and is 1764 cm^{-1} below the ground state dissociation limit. The crossing with $B^2\Sigma_g^+$ occurs at R = 2.222 Å, and lies 2557 cm^{-1} below the same limit.

B Non-Born–Oppenheimer corrections

The derivative coupling $F_{\alpha\beta}$ in eqn (5) is zero unless the colliding particles have different nuclear masses. The evaluation of $F_{\alpha\beta}$ can be conveniently achieved through the expression for its origin dependence.[26,28] The g and u symmetries of the electronic wave functions are labeled according to the center of charge (CC), and the relationship connecting CNM and CC is given by

$$F_{\alpha\beta} = \frac{1}{\mu}\left\langle \psi_\alpha \left| \frac{\partial}{\partial R} \right| \psi_\beta \right\rangle_{\mathrm{CNM}} = \frac{1}{\mu}\left\langle \psi_\alpha \left| \frac{\partial}{\partial R} \right| \psi_\beta \right\rangle_{\mathrm{CC}} + \frac{\eta m_a + (\eta - 1) m_b}{m_a + m_b} \frac{1}{\mu} \langle \psi_\alpha | \nabla_r | \psi_\beta \rangle_{\mathrm{CC}}, \quad (17)$$

where η is the parameter that determines the origin of the coordinate system. For the homonuclear diatomic species $\eta = \frac{1}{2}$. The first term on the right hand side (RHS) of eqn (17) is zero because of the g and u symmetries of the electronic wave functions. The second term is nonzero only if there exists a mass difference between the colliding partners. The calculation of $F_{\alpha\beta}$ becomes the evaluation of the matrix element of the electron velocity operator ∇_r in the CC frame. In the present study, we computed the matrix element using the same MRCISD wave function as in the construction of the PECs. The derived couplings as a function of internuclear distance R are depicted in Fig. 1 for the case of isotopic combination of ^{9}Be and ^{10}Be. In the BO representation $F_{\alpha\beta}$ becomes zero exponentially as $R \to \infty$, which can be seen by transforming $F_{\alpha\beta}$ into the length gauge

$$F_{\alpha\beta} \approx \langle \psi_\alpha | \nabla_r | \psi_\beta \rangle_{\mathrm{CC}} \approx (\varepsilon_\alpha - \varepsilon_\beta) \langle \psi_\alpha | r | \psi_\beta \rangle_{\mathrm{CC}}. \quad (18)$$

The **V** matrix as in eqn (5) contains adiabatic and non-adiabatic corrections to the BO approximation. Accurate accounts of each contributing term expressed in eqn (5) are non-trivial. We have demonstrated[12] that **V** can be accurately determined by directly evaluating the nuclear kinetic operator in the space fixed (SF) frame[47–49] through a numerical differentiation procedure[12]

$$V_{\alpha\beta} = \sum_I^{N_{\mathrm{coord}}} \left\langle \psi_\alpha \left| -\frac{1}{2m_I} \nabla_I^2 \right| \psi_\beta \right\rangle, \quad (19)$$

where the sum runs over the number of nuclear Cartesian coordinates N_{coord}, m_I is the nuclear mass, and ∇_I^2 the Lapacian in Cartesian coordinate I. In our calculation, the molecule was placed in the SF nuclear coordinate frame with the origin placed at the CNM and the z-axis along the molecular axis. The second derivative for each Cartesian coordinate was computed by numerical differentiation at a MCSCF level of theory with a doubly augmented valence quintuple-ζ (d-aug-cc-pV5Z) basis.[39] The active space in this MCSCF wave function was composed of seven electrons in eighteen MOs, formed by 1s2s2p3s3p orbitals of the Be atoms. The accuracy of the MCSCF approach was checked at selected internuclear distances by comparing with those obtained from the MRCISD wave functions. The differences are less than 5%. In addition, a comparison of $F_{\alpha\beta}$ obtained from numerical differentiation with that evaluated through the electron velocity operator according to eqn (17) served as a check on the accuracy of the MCSCF numerical differentiation procedure. Finally, the asymptotic value of the off-diagonal matrix element of **V** can be inferred from atomic calculations combined with atomic spectroscopy, which provide a severe check of our calculation.

In the actual calculation, we directly derive the Hermitian matrix $\tilde{\mathbf{V}}$, given in eqn (7), by computing the overlap of the BO wave functions at displaced nuclear Cartesian coordinates,

$$O_{\alpha\beta}^{\Delta x} = \langle \psi_\alpha(x - \Delta x; R) | \psi_\beta(x + \Delta x; R) \rangle, \quad (20)$$

where x represents the general nuclear Cartesian coordinate and Δx is the displacement. After straightforward algebra,

we obtain for each coordinate I

$$\tilde{V}_{\alpha\beta,I} = \frac{1}{48\Delta x^2}[16(O^{\Delta x}_{\alpha\beta} + O^{\Delta x}_{\beta\alpha}) - (O^{2\Delta x}_{\alpha\beta} + O^{2\Delta x}_{\beta\alpha}) - 30\delta_{\alpha\beta}] + \mathcal{O}(\Delta x^3), \quad (21)$$

and therefore

$$\tilde{V}_{\alpha\beta} = \sum_{I}^{N_{\text{coord}}} -\frac{1}{2m_I}\tilde{V}_{\alpha\beta,I}. \quad (22)$$

Bi-orthogonal molecular orbitals[50] at displaced nuclear configurations were used to calculate the BO overlaps and $\Delta x = 0.005a_0$.

The derived diagonal and off-diagonal matrix elements of $\tilde{\mathbf{V}}$ for the two lowest Σ^+ states of $(^9\text{Be}^{10}\text{Be})^+$ are shown in Fig. 1 as a function of R. They are small quantities and vary slowly as a function of R. Only at very short R, do they become significant. Asymptotically, the diagonal correction is calculated to be 372 cm^{-1} for both states, and the off-diagonal matrix element is determined to be 0.226 cm^{-1}.

The asymptotic off-diagonal matrix element is $\frac{1}{2}\Delta E$, and it causes the two adiabatic states to separate to the correct limits of ($^9\text{Be}^+ + {}^{10}\text{Be}$) and ($^9\text{Be} + {}^{10}\text{Be}^+$) with the former lower in energy. ΔE can be inferred from the high-precision atomic calculations[51,52] and resonance ionization mass spectroscopy.[53] The energy difference in these two limits largely results from the finite mass differences including specific mass shift (SMS) and normal mass shift (NMS). The SMS contribution has been calculated to be 292 MHz (1.2076 μeV),[51] and the experimental value is 270 ± 40 MHz (1.1166 ± 0.1654 μeV).[53] The NMS can be estimated from the atomic calculation with the infinite nuclear mass

$$E_{\text{NMS}} = -\frac{m_e}{m_a + m_e}E(^{\infty}\text{Be}). \quad (23)$$

The nonrelativistic energies for $^{\infty}\text{Be}$ and $^{\infty}\text{Be}^+$ are determined to be −14.6673564631 a.u. and −14.3247631754 a.u. in a recent variational calculation employing explicitly correlated Gaussian functions.[52] According to eqn (23), the NMS difference in the isotopic combination of $(^9\text{Be}^{10}\text{Be})^+$ is 56.4655 μeV. Therefore, $\Delta E \cong 57.67$ μeV. No relativistic and nuclear field effects are considered in our estimate, since they are small for light elements. Our numerical differentiation calculation of $\tilde{V}_{\alpha\beta}$ reproduced this asymptotic result. The accuracy in the numerical differentiation procedure was further checked in the small R region by comparison of the first derivative coupling, given by

$$F^{\text{num}}_{\alpha\beta} = \frac{1}{4\Delta x}(O^{\Delta x}_{\alpha\beta} - O^{\Delta x}_{\beta\alpha}) + \mathcal{O}(\Delta x^2), \quad (24)$$

with the analytical result of $F_{\alpha\beta}$. The two sets of calculations are in good agreement except in the small range ($R < 2.3a_0$), where the numerical noise is large. The difference is normally smaller than 5%.

The electronic orbital angular momentum coupling matrix $\mathbf{L}$ couples Σ^+ and Π states. For the same isotopic combination, only the matrix element between Σ^+_u and Π_u states survives. We computed this coupling matrix element using the same MRCISD wave functions as in the construction of the PECs. In the case of the different isotopic combination, we evaluated these matrix elements using the MCSCF(7e, 18o) wave function as in the calculation of $\tilde{\mathbf{V}}$. Benchmark calculations at selected R showed that the MCSCF results agree closely with the one obtained from MRCISD wave functions. Asymptotically, the couplings approach zero because the Be(^{1}S) → Be(^{3}P) transition is spin-forbidden. As $R \to \infty$, the electronic basis $|\psi\rangle$ becomes an atomic eigenfunction, and the matrix element is given by[28,54]

$$\langle\psi_\Lambda|iL_y|\psi_{\Lambda\pm1}\rangle \approx R(\varepsilon_{\Lambda\pm1} - \varepsilon_\Lambda)\langle\psi_\Lambda|x^{\text{at}}|\psi_{\Lambda\pm1}\rangle_\infty + \langle\psi_\Lambda|iL^{\text{at}}_y|\psi_{\Lambda\pm1}\rangle_\infty, \quad (25)$$

where terms on the RHS with the superscript "at" refer to atom-centered operators. The computed couplings for $(^9\text{Be}^{10}\text{Be})^+$ are plotted in Fig. 1. Similar to the mass dependence in $F_{\alpha\beta}$, the coupling between Σ^+_g and Π_u (for convenience in the discussion, we keep the g and u labelings for the isotopic combination) is weak in the whole range of R.

MOLPRO 2009.1[55] suite of quantum chemistry programs was employed for all of the MRICSD and MCSCF calculations.

IV. Results and discussion

A Near resonance and resonance charge exchange

Scattering calculations have been carried out for collision energies from 10^{-12} eV to 0.5 eV. In the case of near resonance charge exchange (NRCE), the scattering energy is measured from the second channel of $^9\text{Be} + {}^{10}\text{Be}^+$, whose asymptotic energy was set at 5.767×10^{-5} eV above the lowest limit of $^9\text{Be}^+ + {}^{10}\text{Be}$. The PEC of the $A^2\Pi$ state was shifted (~ 5 cm^{-1}) to match the asymptotic energy separation to the experimental value of 2.724 eV[56] between Be(^{1}S) and Be(^{3}P). The computed cross sections for the NRCE processes are shown in Fig. 2. The inelastic exothermic process

$$^9\text{Be} + {}^{10}\text{Be}^+ \to {}^9\text{Be}^+ + {}^{10}\text{Be}$$

is described as "quenching" in Fig. 2. At low collision energies ($< 10^{-8}$ eV), the quenching cross section exhibits the inverse velocity dependence behavior of Wigner's threshold law.[57]

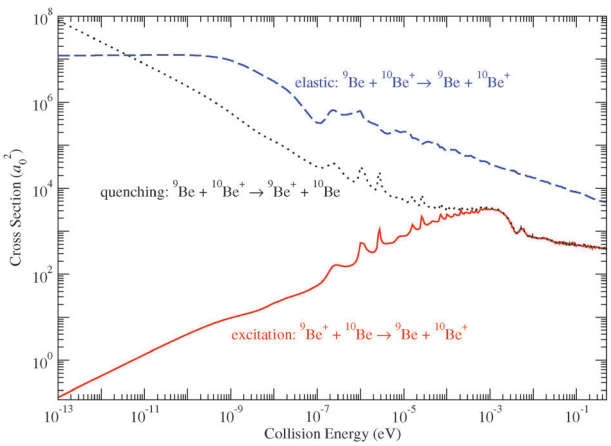

Fig. 2 Charge exchange and elastic cross sections for $(^9\text{Be} + {}^{10}\text{Be})^+$ as a function of collision energy measured from the $^9\text{Be} + {}^{10}\text{Be}^+$ threshold.

Table 3 Scattering length (atomic units) for resonance and near resonance charge exchange collisions. The number next to β is the limiting value of zero temperature quenching rate constant in $cm^3\ s^{-1}$

System	α	β/rate
$^9Be + {}^{10}Be^+ \rightarrow {}^9Be^+ + {}^{10}Be$	−981.4	$50.3/4.5 \times 10^{-10}$
System	$a_g\ (B^2\Sigma_g^+)$	$a_u\ (\tilde{X}^2\Sigma_u^+)$
$^9Be + {}^9Be^+$	−941.8	569.4
$^{10}Be + {}^{10}Be^+$	−229.2	1237.0

According to microscopic reversibility, the reverse endothermic excitation process consequently has a cross-section that approaches zero at the threshold ΔE. The elastic cross section tends to a constant. The zero energy collisions can be characterized by a complex scattering length,[58] $\alpha - i\beta$, the imaginary part of which is related directly to the inelastic cross section. The derived complex scattering length from the S matrix at near zero incident energy is reported in Table 3. The real and negative scattering length of −981.4 a.u. indicates the absence of a near zero energy bound state.

The rate constant for the quenching reaction at zero temperature limit is determined to be $4.5 \times 10^{-10}\ cm^3\ s^{-1}$. Compared to similar quenching reactions in the ion–atom collisions of H and Li with their isotopes,[11,12] this rate is smaller. We have shown that the comparable quenching rates in HD^+ and $^6Li^7Li^+$ were the result of the balance between the smaller threshold energy ΔE and the weaker non-adiabatic couplings. The reduced charge exchange rate is mainly due to the larger mass of the Be atoms: if we assume that the mass independent terms in eqn (17) are nearly the same for Li and Be cases, we see that the increase in the nuclear mass reduces the non-adiabatic coupling term by about 40% and the energy separation only by 20%. Therefore in the present situation, the elastic process is always dominant except at very low energies, $E < 10^{-11}$ eV (which corresponds to a temperature of 10^{-7} K).

Resonance charge exchange (RCE) occurs together with NRCE in an ensemble of mixed isotopes. The computed cross sections for $^9Be_2^+$ and $^{10}Be_2^+$ are presented on the left in Fig. 3 together with one of NRCE (same data as Fig. 2) for comparison.

The overall behavior of the cross section is similar to what has been found in our previous calculations,[11,12] but the details depend on the interaction potentials and particularly on the position of the last bound state in the potential well at very low energy. In the present case, the RCE cross sections for ^9Be and ^{10}Be are close to each other in the whole energy range. They dominate over the NRCE process in a wide energy range from 10^{-3} eV to 10^{-10} eV, and they tend to constants at low energies. The derived scattering lengths, a_g and a_u, for the Σ_g^+ and Σ_u^+ potentials and for the two isotopes are listed in Table 3. Both isotopes show a negative scattering length for the $B^2\Sigma_g^+$ state.

For collision energies above 10^{-3} eV, which is about two orders of magnitude larger than the threshold energy of $(^9Be^{10}Be)^+$, the cross sections for the three charge exchange processes are very much the same. The cross sections vary as $(a \ln E - b)^2$, reflecting the exponential decay of the exchange energy at large R.[24] a and b are determined to be 1.4 a_0 and 18.7 a_0 with E measured in electron volts and σ_{cx} in units of a_0^2. This result is consistent with isotopic ion–atom collisions in H and Li.[11,12]

The elastic cross sections are reported on the right panel in Fig. 3 for both NRCE and RCE processes and are seen to be quite similar for $E > 10^{-5}$ eV. They can be well described by the semiclassical theory and vary as $\sim(\mu C_4^2/E)^{1/3}$.[10,24] For low energies, they become constants, whose magnitudes are governed by the last bound state of the interaction potential and are characterized by the scattering lengths in Table 3.

With the computed charge exchange cross sections, we evaluated the thermally averaged charge exchange rate constants, and the results are plotted in Fig. 4 as a function of temperature. As $T \rightarrow 0$, the rate coefficient of NRCE approaches a constant because the cross section varies inversely as the relative velocity. On the other hand, the RCE rate tends to zero because of the elastic nature of the process. In a wide temperature range, $T \approx$ μK–K, the rate of NRCE is smaller than those of the RCE because of the small cross section. At high temperatures, the rate coefficients of RCE and NRCE processes are indistinguishable. In the NRCE, the rate constant

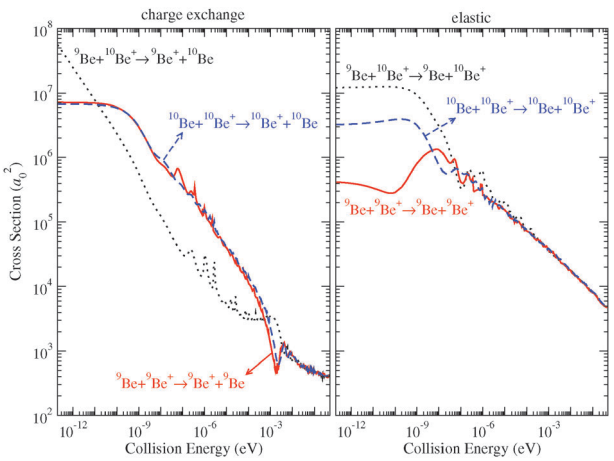

Fig. 3 Charge exchange (left) and elastic (right) cross sections of near resonance and resonance as a function of collision energy. The collision energy in the near resonance case is measured with respect to the $^9Be + {}^{10}Be^+$ threshold.

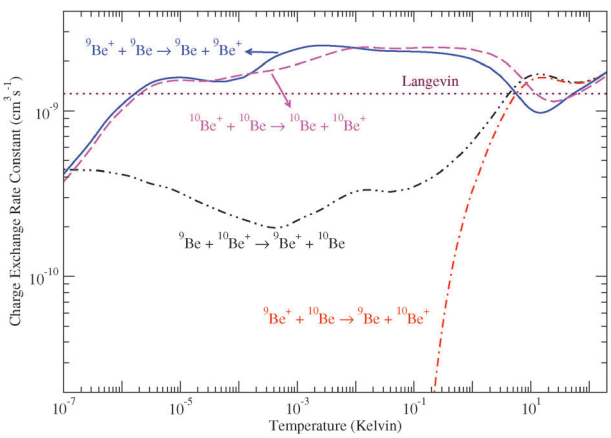

Fig. 4 Thermal rate constants of the charge exchange processes for ion–atom collisions of Be isotopes as functions of temperature. The Langevin rate constant is evaluated for the reduced mass of $^9Be + {}^{10}Be^+$.

of the excitation process decreases significantly as the temperature decreases, and becomes negligible ($<10^{-17}$ cm^3 s^{-1}) for $T < 0.04$ K. According to the microscopic reversibility, the quenching rate coefficient (k_q) and the excitation rate coefficient (k_e) are related by

$$k_q = k_e e^{-\Delta E/k_B T} \quad (26)$$

where k_B is the Boltzmann constant. The rate coefficients evaluated by eqn (26) are consistent with those derived from the computed excitation cross sections.

We have shown previously[10,12,13,24] that the Langevin charge exchange model is successful in the intermediate energy range. The semiclassical Langevin model assumes that every collision whose energy overcomes the centrifugal barrier penetrates to sufficiently small distances to form a complex that leads to reaction with a probability of order unity.[59] The rate coefficient for the R^{-4} potential is $\pi\sqrt{2C_4/\mu}$, which is independent of temperature and has a weak dependence on the reduced mass. The rate coefficient of NRCE at low energies is also independent of temperature, but it is governed by the s-wave scattering, which sensitively depends on the details of the interaction potential and the reduced mass. In the present case, for ^{9}Be atoms undergoing charge exchange with ^{10}Be$^+$, the Langevin rate coefficient is 1.27×10^{-9} cm^3 s^{-1}. It is plotted in Fig. 4 for comparison. For the NRC, the quantum mechanical rate coefficients are close to the Langevin value in a broad temperature range from 100 K down to mK. However, the Langevin result is always larger than that of the NRCE except in a limited temperature range of 1 K–100 K. Overall, these results agree with our previous findings. While the agreement between the Langevin model and quantum mechanical results is close, large discrepancies may exist, *e.g.* the RCE of ^{6}Li + ^{6}Li^{+12} and ^{171}Yb + ^{171}Yb^{+13} and the NRCE of ^{9}Be + ^{10}Be$^+$. Care must be taken when applying the Langevin formula, especially at low energies.

B The influence of the Π state

The main difference with our previous studies[10–13] of other similar systems is that, here, a third state, $A^2\Pi$, is directly involved in both the RCE and NRCE processes. In the former case, the $A^2\Pi_u$ state interacts only with $\tilde{X}^2\Sigma_u^+$ because of the g/u inversion symmetry, while it couples both Σ states in the latter case. To explore its role in the charge exchange processes, we performed model studies by removing the $A^2\Pi$ state and the corresponding electronic orbital angular momentum couplings from the coupled eqn (6). The computed elastic and charge exchange cross sections are compared with those obtained from the full three-state calculations. The differences in the charge exchange cross sections are expressed as the percentage deviation from the results of the full calculations, and are plotted in Fig. 5 as a function of collision energy for NRCE and RCE processes, respectively. A similar situation occurs for the elastic cross sections, but it is not shown for brevity.

For the charge exchange cross sections, the $A^2\Pi$ state plays a negligible role for scattering energies smaller than 10^{-6} eV. The percentage difference is much smaller than 0.1%. There are various causes for this behavior: first of all, the non-adiabatic interaction between the $A^2\Pi$ and $^2\Sigma^+$ states is weak.

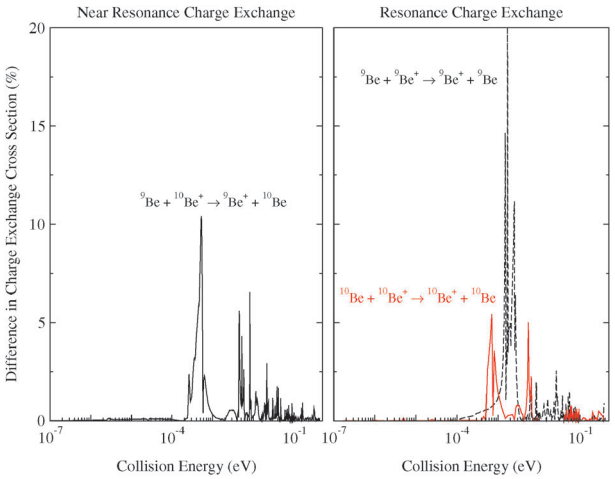

Fig. 5 The percentage differences of the charge exchange cross sections as a function of collision energy obtained from the calculations with and without the $A^2\Pi_u$ state for the near resonance (left) and resonance (right) charge exchange processes.

At the crossing region its magnitude is on the order of 10^{-5} a.u. Secondly, in the low energy regime, the inner region of the $B^2\Sigma^+$ state is inaccessible because of the potential barrier of 1260 cm^{-1} (see Fig. 6). The crossing between the $A^2\Pi$ state and $\tilde{X}^2\Sigma^+$ state at $R_c = 3.015a_0$ is located 1746 cm^{-1} below the maxima in the $B^2\Sigma^+$ potential. Furthermore, for an R^{-4} potential the scattering phase shift at low energies is dominated by the long-range part of the interaction potentials. The shape of the potential well region makes only a minor contribution. This can be easily verified by manipulating the inner part of the potential of the $\tilde{X}^2\Sigma^+$ state. When we set this potential to be a constant for $R < 2.9a_0$ arbitrarily larger or smaller of ±200 cm^{-1} than its value at $R = 2.9a_0$, we noticed that the phase shifts coming from this modified potential did not differ significantly from those coming from the actual potential at few selected energies from 10^{-10} eV to 10^{-7} eV. We found, in particular, that the variation of the module of the phase shifts was smaller than 1% depending on the collision energy. Therefore, the charge exchange cross sections at low energies are largely insensitive to the $A^2\Pi$ state, and so are the elastic cross sections.

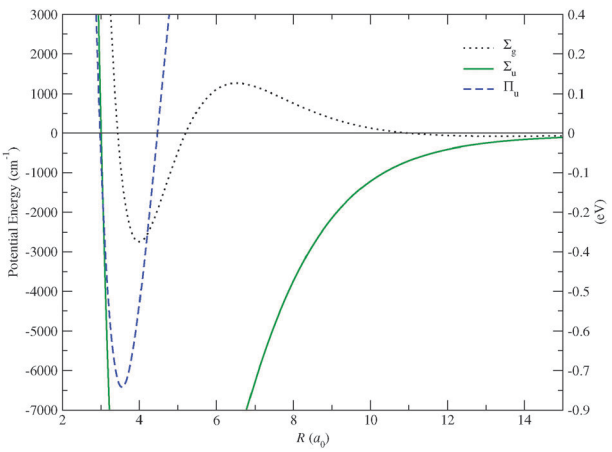

Fig. 6 BO potentials in the short R region.

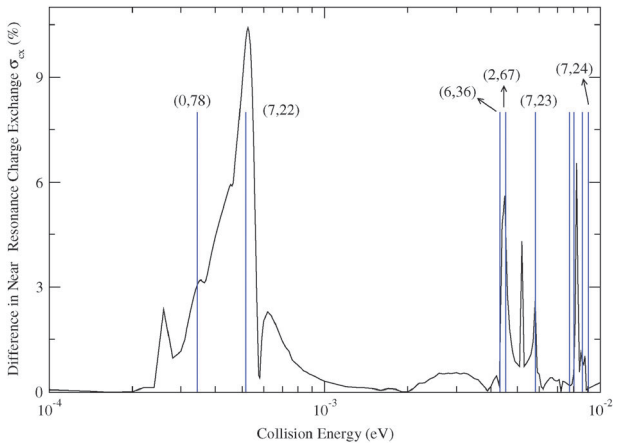

Fig. 7 The percentage differences of the charge exchange cross sections as a function of collision energy obtained from the calculations with and without the $A^2\Pi_u$ state for the near resonance charge exchange processes. The vertical lines represent selected ro-vibrational levels of the $A^2\Pi_u$ state, and their positions are relative to the $^9Be + {}^{10}Be^+$ limit. These levels are characterized by the vibrational (ν) and rotational quantum number (J), which are shown in the parenthesis as (ν, J).

Relatively large discrepancies between the calculations including the Π state or not start to appear when $E > 10^{-4}$ eV. The difference remains small and does not exceed 20% in the sampled interval of scattering energies. The differences are mainly caused by Feshbach resonances due to the presence of quasi-bound states of the $A^2\Pi$ potentials embedded in the Σ continuum. In Fig. 7, we show the positions of a few selected bound states of the $A^2\Pi$ state of $(^9Be^{10}Be)^+$. Their positions coincide with the peaks in the difference of the cross section, identifying the energies where the Σ–Π interaction is enhanced by this resonant mechanism. At collision energies below 10^{-4} eV, no bound state is found to be in resonance with the incoming wave.

V. Summary and conclusions

We have investigated slow collisions of a Be atom with a Be ion including the case of different isotopes. High-level electronic structure calculations at the MRCISD and MCSCF levels of theory have been performed to construct the Born–Oppenheimer molecular potentials and the diagonal and off-diagonal corrections that reflect the breakdown of the BO approximation. The calculated potential energy curves agree closely with recent experiments and theoretical analysis. The computed energy splitting of $\Delta E = 56.47$ μeV in the isotopic combination of the $(^9Be^{10}Be)^+$ molecular ion is consistent with the result of 57.76 μeV derived from high precision atomic calculations and resonance ionization mass spectroscopy.

Close-coupling calculations have been carried out to examine the collision dynamics of resonance and near resonance charge exchange. We have demonstrated that the NRCE cross section in the low-energy limits follows Wigner's threshold law, varying as the inverse of the initial velocity. The limiting charge exchange rate coefficient is determined to be 4.5×10^{-10} cm^3 s^{-1}. In comparison, the resonance charge exchange rate tends to zero. When the collision energy is much higher than the threshold energy arising from the isotope shift, NRCE becomes identical to RCE. Close agreement with the Langevin charge model is found over a wide energy range. These results are consistent with findings in our earlier investigations of the isotopic ion–atom collision of HD^+ [11] and Li_2^+.[12]

A key aspect of the present work was to explore the perturbation, originating from the non-adiabatic interaction with a Π state, to the two-state approximation for the description of ion–atom collisions. Our theoretical analysis showed that in the low energy regime, the effects due to the Π state on the elastic and the charge exchange processes in both NRCE and RCE cases are negligible. Not only because the Π–Σ coupling is weak, but more importantly, because the low energy scattering dynamics is dominated by the strong long-range polarization interaction. The majority of the scattering phase is accumulated in the long-range part of the potential. The contribution from the short range is small and insensitive to the details of the interaction potentials. Above 0.1 meV of collision energy, the effects due to the Π state are still relatively small and mainly caused by the appearance of Feshbach resonances due to the presence of quasi-bound states of the Π state. Of course, if there existed quasi-bound states at suitable positions, this type of resonances could also take place below 0.1 meV. Nonetheless, we have explicitly checked that the two-state approximation for the slow ion–atom collision is largely valid even in this case.

Acknowledgements

This research was partly supported by the Chemical Sciences, Geosciences and Biosciences Division of the Office of Basic Energy Science, Office of Science, US Department of Energy and partly by the NSF through the Harvard-MIT Center for Ultracold Atoms (AD and PZ). EB acknowledges travel support from the Institute for Theoretical Atomic, Molecular, and Optical Physics which is funded by the NSF. RC was supported by the NSF grant (0653449). We are grateful for the valuable discussions with Prof. V. Kharchenko.

References

1 L. D. Carr, D. DeMille, R. V. Krems and J. Ye, *New J. Phys.*, 2009, **11**, 055049.
2 H. L. Bethlem and G. Meijer, *Int. Rev. Phys. Chem.*, 2003, **22**, 73.
3 J. Doyle, B. Friedrich, R. V. Krems and F. Masnou-Seeuws, *Eur. Phys. J. D*, 2004, **31**, 149.
4 T. Schneider, B. Roth, H. Duncker, I. Ernsting and S. Schiller, *Nat. Phys.*, 2010, **6**, 275.
5 X. Tong, A. H. Winney and S. Willitsch, *Phys. Rev. Lett.*, 2010, **105**, 143001.
6 S. Schmidt, A. Härter and J.-H. Denschlag, *Phys. Rev. Lett.*, 2010, **105**, 133202.
7 A. T. Grier, M. Cetina, F. Oručević and V. Vuletić, *Phys. Rev. Lett.*, 2009, **102**, 223201.
8 B. Gao, *Phys. Rev. Lett.*, 2010, **104**, 213201.
9 P. Raab and H. Friedrich, *Phys. Rev. A: At., Mol., Opt. Phys.*, 2009, **80**, 052705.
10 R. Côté and A. Dalgarno, *Phys. Rev. A: At., Mol., Opt. Phys.*, 2000, **62**, 012709.
11 E. Bodo, P. Zhang and A. Dalgarno, *New J. Phys.*, 2008, **10**, 033024.
12 P. Zhang, E. Bodo and A. Dalgarno, *J. Phys. Chem. A*, 2009, **113**, 15085.
13 P. Zhang, R. Côté and A. Dalgarno, *Phys. Rev. A: At., Mol., Opt. Phys.*, 2009, **80**, 030703(R).
14 C. Zipkes, S. Palzer, L. Ratschbacher, C. Sias and M. Köhl, *Phys. Rev. Lett.*, 2010, **105**, 133201.

15 Z. Idziaszek, T. Calarco, P. S. Julienne and A. Simoni, *Phys. Rev. A: At., Mol., Opt. Phys.*, 2009, **79**, 010702.
16 S. Willitsch, M. T. Bell, A. D. Gingell and T. P. Softley, *Phys. Chem. Chem. Phys.*, 2008, **10**, 7200.
17 D. I. Schuster, L. S. Bishop, I. L. Chuang, D. DeMille and R. J. Schoelkopf, *Phys. Rev. A: At., Mol., Opt. Phys.*, 2011, **83**, 012311.
18 A. André, D. DeMille, J. M. Doyle, M. D. Lukin, S. E. Maxwell, P. Rabl, R. J. Schoelkopf and P. Zoller, *Nat. Phys.*, 2006, **2**, 636.
19 A. Micheli, G. K. Brennen and P. Zoller, *Nat. Phys.*, 2006, **2**, 341.
20 V. V. Flambaum and M. G. Kozlov, *Phys. Rev. Lett.*, 2007, **99**, 150801.
21 F. M. Cucchietti and E. Timmermans, *Phys. Rev. Lett.*, 2006, **96**, 210401.
22 R. Côté, *Phys. Rev. Lett.*, 2000, **85**, 5316.
23 R. Côté, V. Kharchenko and M. D. Lukin, *Phys. Rev. Lett.*, 2002, **89**, 930011.
24 A. Dalgarno, *Philos. Trans. R. Soc. London, Ser. A*, 1958, **250**, 426.
25 R. T. Pack and J. O. Hirschfelder, *J. Chem. Phys.*, 1968, **49**, 4009.
26 T. G. Heil, S. E. Butler and A. Dalgarno, *Phys. Rev. A: At., Mol., Opt. Phys.*, 1981, **23**, 1100.
27 J. Grosser, *Z. Phys. D: At., Mol. Clusters*, 1986, **3**, 39.
28 A. K. Belyaev, A. Dalgarno and R. McCarroll, *J. Chem. Phys.*, 2002, **116**, 5395.
29 V. I. Tselyaev, *J. Comput. Appl. Math.*, 2004, **170**, 103.
30 B. R. Johnson, *J. Chem. Phys.*, 1978, **69**, 4678.
31 I. Fischer, V. E. Bondybey, P. Rosmus and H.-J. Werner, *Chem. Phys.*, 1991, **151**, 295.
32 H. Hogreve, *Chem. Phys. Lett.*, 1991, **187**, 479.
33 S. Banerjee, J. N. Byrd, R. Côté, H. H. Michels and J. A. Montgomery Jr., *Chem. Phys. Lett.*, 2010, **496**, 208.
34 I. O. Antonov, B. J. Barker, V. E. Bondybey and M. C. Heaven, *J. Chem. Phys.*, 2010, **133**, 074309.
35 H.-J. Werner and P. J. Knowles, *J. Chem. Phys.*, 1988, **89**, 5803.
36 S. R. Langhoff and E. R. Davidson, *Int. J. Quantum Chem.*, 1974, **8**, 61.
37 H.-J. Werner and P. J. Knowles, *J. Chem. Phys.*, 1985, **82**, 5053.
38 A. Wolf, M. Reiher and B. A. Hess, *J. Chem. Phys.*, 2002, **117**, 9215.
39 B. P. Prascher, D. E. Woon, K. A. Peterson, T. H. Dunning and A. K. Wilson, *Theor. Chem. Acc.*, 2011, **128**, 69.
40 M. P. de Lara-Castells, R. V. Krems, A. A. Buchachenko, G. Delgado-Barrio and P. Villarreal, *J. Chem. Phys.*, 2001, **115**, 10438.
41 K. T. Tang and J. P. Toennies, *J. Chem. Phys.*, 1984, **80**, 3726.
42 A. Derevianko, S. G. Porsev and J. F. Babb, *At. Data Nucl. Data Tables*, 2010, **96**, 323.
43 J. R. Hammond1, K. Kowalski and W. A. deJong, *J. Chem. Phys.*, 2007, **127**, 144105.
44 M. Valiev, E. J. Bylaska, N. Govind, K. Kowalski, T. P. Straatsma, H. van Dam, D. Wang, J. Nieplocha, E. Apra and T. L. Windus, *et al.*, *Comput. Phys. Commun.*, 2010, **181**, 1477.
45 J. Mitroy, *Phys. Rev. A: At., Mol., Opt. Phys.*, 2010, **82**, 052516.
46 D. Sundholm and J. Olsen, *Phys. Rev. A: At., Mol., Opt. Phys.*, 1993, **47**, 2672.
47 N. C. Handy, Y. Yamaguchi and H. F. Schaefer, *J. Chem. Phys.*, 1986, **84**, 4481.
48 H. Sellers and P. Pulay, *Chem. Phys. Lett.*, 1984, **103**, 463.
49 W. Kutzelnigg, *Mol. Phys.*, 1997, **90**, 909.
50 A. Mitrushchenkov and H.-J. Werner, *Mol. Phys.*, 2007, **105**, 1239.
51 J. Komasa, W. Cencek and J. Rychlewski, *Phys. Rev. A: At., Mol., Opt. Phys.*, 1995, **52**, 4500.
52 M. Stanke, D. Kdziera, S. Bubin1 and L. Adamowicz, *Phys. Rev. A: At., Mol., Opt. Phys.*, 2007, **75**, 052510.
53 J. Wen, J. C. Travis, T. B. Lucatorto, B. C. Johnson and C. W. Clark, *Phys. Rev. A: At., Mol., Opt. Phys.*, 1988, **37**, 4207.
54 J. Grosser, T. Menzel and A. K. Belyaev, *Phys. Rev. A: At., Mol., Opt. Phys.*, 1999, **59**, 1309.
55 H.-J. Werner, P. J. Knowles, F. R. Manby and M. Schütz, *et al.*, *Molpro, version 2009.1, a package of ab initio programs*, 2009, http://www.molpro.net.
56 Y. Ralchenko, A. Kramida, J. Reader and N. A. Team, *NIST Atomic Spectra Database (ver. 4.0.1)*, NIST, 2011.
57 E. P. Wigner, *Phys. Rev.*, 1948, **73**, 1002.
58 N. Balakrishnan, V. Kharchenko, R. C. Forrey and A. Dalgarno, *Chem. Phys. Lett.*, 1997, **280**, 5.
59 P. Langevin, *Ann. Chim. Phys.*, 1905, **5**, 245.